Arch. Mech., 36, 2, pp. 241–250, Warszawa 1984

Computer simulation of convection in floating zone melting(*)

S. G. SLAVTCHEV and J. D. KOJUKHAROVA (BAS)

SURFACE-TENSION driven flow in a noncylindrical melting zone suspended between two rods has been investigated by a numerical solution of the Navier–Stokes equations with the Boussinesq approximation and the heat transfer equation. The shape of the free surface is determined from the force balance on it, provided the fluid is in a quasi-equilibrium state. The gravity is taken into account. The influence of the convection and the zone geometry on the temperature distribution for different Marangoni numbers is shown.

Przepływ wywołany napięciem powierzchniowym w niecylindrycznej strefie topnienia zawieszonej między dwoma prętami zanalizowano, rozwiązując numerycznie równanie Naviera–Stokesa w przybliżeniu Boussinesqa oraz równanie przewodnictwa ciepła. Kształt powierzchni swobodnej określono z warunku równowagi sił zakładając, że płyn znajduje się w stanie quasi-równowagi. Uwzględniono siły ciężkości. Pokazano wpływ konwekcji i geometrii strefy topnienia na rozkład temperatury przy różnych wartościach liczby Marangoniego.

Течение, вызванное поверхностным натяжением в нецилиндрической плавающей зоне, подвешенной между двумя стержнями, анализируется, решая численно уравнения Навье-Стокса в приближении Буссинеска и уравнение теплопроводности. Форма свободной поверхности определена из условия равновесия сил, предполагая, что жидкость находится в состоянии квазиравновесия. Учтена сила тяжести. Показано влияние конвекции и геометрии плавающей зоны на распределение температуры, при разных значениях числа Марангони.

Nomenclature

a_r, a_φ, a_z functions defined in Table 1,
A aspect ratio of the zone,
b_φ function defined in Table 1,
d_φ function defined in Table 1,
F dimensionless equation of the free surface,
g acceleration due to gravity,
L half zone length,
p^0 constant,
r dimensionless radial coordinate,
$\tilde{r}$ transformed radial coordinate,
R zone radius,
T temperature,
T_{max} maximum temperature at the free surface,
T_s temperature of the rods,
ΔT $T_{max} - T_s$,
z dimensionless axial coordinate.

Greek symbols

α temperature coefficient of the surface tension, $\left|\frac{\partial \sigma}{\partial T}\right|$,
β thermal expansion coefficient,

(*) Paper given at XVI Symposium on Advanced Problems and Methods in Fluid Mechanics, Spała, 4–10 September, 1983.

γ_1, γ_2 contact angles at the lower and upper rods,
θ dimensionless temperature,
$\bar{\theta}$ dimensionless temperature at the free surface,
ν kinematic viscosity,
ϱ density,
σ surface tension,
φ function defined in Table 1,
χ thermal diffusivity,
ψ dimensionless stream function,
ω dimensionless vorticity.

1. Introduction

A FLOATING-ZONE technique is widely used to produce high purity crystals for special electronic devices. For example, the floating zone melting is used to grow silicon and germanium crystals [1]. It is of some importance for the growth of high melting point materials such as W, Mo, Al_2O_3 etc.

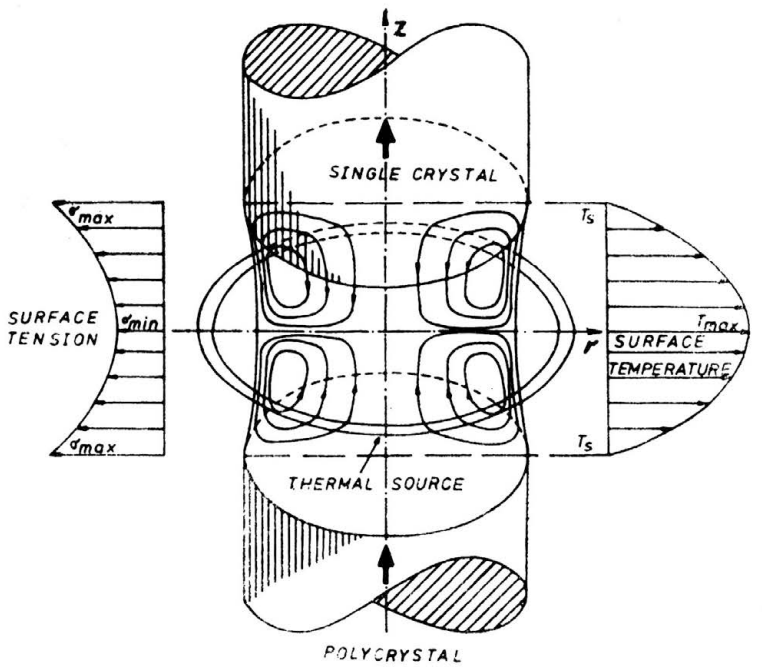

FIG. 1.

The technique is shown schematically in Fig. 1. A molten zone is established between two rods, a charge (or feed) rod of polycrystalline material and a crystalline rod, and held by capillary forces. Heating is concentrated at the middle equator plane. By moving the crystal up, the zone travels through the crystal.

Convection in the zone is generally driven by buoyant forces, surface tension forces due to temperature gradients existing along the free surface, movement of the zone through

the solid and rotations of the rods. It plays an important role in impurity distribution in crystals purified by the zone melting method and has been intensively studied both experimentally [2–13] and theoretically [14–22] in the last decade. A critical review of results obtained has been done by SCHWABE [23].

In the case of no rotation the model experiments with $NaNO_3$ [3, 5], KCl [5] and methyl alcohol [8, 10] and the numerical calculations [17–19] show the importance of surface tension forces, e.g. of Marangoni effects. The thermocapillary flow is dominating over the buoyancy-driven flow for small liquid zones and the zone movement has a negligibly small influence on the convection. For small temperature gradients the flow patterns observed are qualitatively the same as calculated. For larger gradients experimental results (see for example, [3, 9]) differ from theoretical ones (say [14, 15, 19]). At larger values of Marangoni numbers the axisymmetric numerical calculations predict the development of secondary vortex cells, while the experiments show a nonaxisymmetric distortion and oscillation (or rotation) of the primary cell formed in a half-zone [4, 9]. This difference might be explained by the limitation of the numerical results in their applicability by the assumption of an ideal cylindrical zone and idealized temperature distributions along the melt surface. Moreover, the experiments were performed using a half-zone heated above instead of a full zone heated in the middle. As it is first pointed by CLARK and WILCOX [18], the difference between temperature conditions in experiments and calculations might prove crucial. Forced convection due to crystal rotation has been numerically studied in [16, 20, 21].

In the present paper a convection flow due to surface tension and buoyant forces in a noncylindrical zone is theoretically investigated. The shape of the free surface is approximated by a static meniscus and the axisymmetrical domain is transformed into a cylindrical one. Then, transformed steady state equations for momentum and heat transfer are solved by the integro-interpolating method [24]. Calculations are carried out for a parabolic temperature profile at the free surface of the melt corresponding to radiant heating in the zone equator plane.

It is shown that the gravity has a negligible effect on the convection as well as on the temperature distribution in the small zones considered. The convection flow influences strongly the temperature field. Due to the stronger vorticity of the liquid in an axisymmetric zone, the temperature distribution differs considerably from that in a cylindrical one, especially in the core. The convective heat transfer dominates at larger Marangoni numbers and/or larger Prandtl numbers.

2. Mathematical model

An incompressible axisymmetric steady state flow in the liquid zone placed between two rods is assumed, with constant properties. Under the gravity the shape of the free surface is not cylindrical but it is approximately axisymmetric. We assume that the shape deviates slightly from that in the case of equilibrium state, without crystal rotation.

Let the radii of the rods be equal to R and the zone length be $2L$. In a cylindrical coordinate system r, z (Fig. 1) the dimensionless governing equations in the stream function

ψ and the vorticity ω variables and the equation for the temperature $\theta = (T-T_s)/\Delta T$ are as follows (all symbols are defined in the table of nomenclature):

$$(2.1)\quad r^2\left[\frac{\partial}{\partial z}\left(\frac{\omega}{r}\frac{\partial\psi}{\partial r}\right)-\frac{\partial}{\partial r}\left(\frac{\omega}{r}\frac{\partial\psi}{\partial z}\right)\right] - \frac{1}{\mathrm{Re}}\left\{\frac{\partial}{\partial z}\left[r^3\frac{\partial}{\partial z}\left(\frac{\omega}{r}\right)\right]+\frac{\partial}{\partial r}\left[r^3\frac{\partial}{\partial r}\left(\frac{\omega}{r}\right)\right]\right\}+\frac{\mathrm{Gr}}{\mathrm{Re}^2}r^2\frac{\partial\theta}{\partial r}=0,$$

$$(2.2)\quad \omega = -\left[\frac{\partial}{\partial z}\left(\frac{1}{r}\frac{\partial\psi}{\partial z}\right)+\frac{\partial}{\partial r}\left(\frac{1}{r}\frac{\partial\psi}{\partial r}\right)\right],$$

$$(2.3)\quad \frac{\partial}{\partial z}\left(\theta\frac{\partial\psi}{\partial r}\right)-\frac{\partial}{\partial r}\left(\theta\frac{\partial\psi}{\partial z}\right)-\frac{1}{\mathrm{Pr}\,\mathrm{Re}}\left[\frac{\partial}{\partial z}\left(r\frac{\partial\theta}{\partial z}\right)+\frac{\partial}{\partial r}\left(r\frac{\partial\theta}{\partial r}\right)\right]=0.$$

Here $\mathrm{Gr} = g\beta\Delta TL^3/\nu^2$ is the Grashoff number, $\mathrm{Re} = \alpha\Delta TL/\nu^2\varrho$ the Reynolds number and $\mathrm{Pr} = \nu/\chi$ the Prandtl number. The coordinates, stream function, vorticity and temperature are related to L, $\alpha\Delta TL^2/\nu\varrho$, $\alpha\Delta T/\varrho\nu\,L$, $\Delta T = T_{\max}-T_s$, respectively. The boundary conditions are:

a) $z = \pm 1$ (at the rods)

$$(2.4)\quad \psi = \frac{\partial\psi}{\partial z} = 0, \quad \theta = 0;$$

b) $r = 0$ (axis)

$$(2.5)\quad \psi = \frac{\partial\psi}{\partial r} = 0, \quad \frac{\partial\theta}{\partial r} = 0;$$

c) $r = F(z)$ (free surface)

$$(2.6)\quad \psi = 0, \quad \theta = \tilde{\theta}(z),$$

$$-\omega = -\frac{(1+F'^2)^{1/2}}{1-F'^2}\frac{\partial\tilde{\theta}}{\partial z}+\frac{2}{F}\frac{\partial^2\psi}{\partial z^2}+\frac{4F'}{F(1-F'^2)}\left[\frac{\partial^2\psi}{\partial r\,\partial z}-\frac{1}{2F}\frac{\partial\psi}{\partial z}\right].$$

Here a prime denotes differentiation with respect to z. The thermocapillary convection is characterized by the Marangoni number $\mathrm{Ma} = \alpha\Delta TL/\varrho\nu\chi = \mathrm{RePr}$. The ratio between the buoyant force on a volume and the surface tension force on the surface element in the volume is called the dynamic Bond number

$$(2.7)\quad \mathrm{Bo}_{\mathrm{dyn}} = \frac{\mathrm{Gr}}{\mathrm{Re}} = \frac{\varrho g\beta L^2}{\alpha}$$

and $\mathrm{Bo}_{\mathrm{dyn}} < 1$ is a criterion for the dominance of the thermocapillary convection.

When the fluid is in an equilibrium state under gravity the zone length is limited and depends on the balance between the surface tension forces and the hydrostatic pressure. The maximum stable length as well as the stable zone shape depends on the static Bond number $\mathrm{Bo}_{\mathrm{stat}} = \varrho gL^2/\sigma$, which is the ratio of these two forces. The shape of the molten quasi-static zone is determined from the Laplace equation

$$(2.8)\quad \frac{F''}{(1+F'^2)^{3/2}}-\frac{1}{F(1+F'^2)^{1/2}}+p^0-\mathrm{Bo}_{\mathrm{stat}}z=0,$$

where p^0 is an unknown constant. The boundary conditions for the equation are

$$F = A, \quad -\frac{F'}{(1+F'^2)^{1/2}} = \cos\gamma_1 \quad \text{at} \quad z = -1,$$
$$\frac{F'}{(1+F'^2)^{1/2}} = \cos\gamma_2 \quad \text{at} \quad z = 1. \tag{2.9}$$

At given γ_1, γ_2 and A the shape and the radius of the upper rod depend on the static Bond number. Stability of liquid zones with different radii of the rods is studied, for example, in [25]. The book [26] is partially dedicated to problems connected with the equilibrium shape of a liquid.

3. Computation

The momentum and heat transfer equations are solved by the integro-interpolating method (see, for example, [24]). First, the zone is transformed into a cylinder by the transformation

$$\tilde{r} = \frac{r}{F(z)}. \tag{3.1}$$

In the new coordinates $\tilde{r}$, z Eqs. (2.1)–(2.3) can be presented by a model equation

$$a_\varphi\left[\frac{\partial}{\partial z}\left(\varphi a_r \frac{\partial\psi}{\partial\tilde{r}}\right) - a_r\frac{\partial}{\partial\tilde{r}}\left(\varphi\frac{\partial\psi}{\partial z}\right)\right] + a_\varphi\left[a_z\frac{\partial}{\partial\tilde{r}}\left(\varphi a_r\frac{\partial\psi}{\partial\tilde{r}}\right) - a_r\frac{\partial}{\partial\tilde{r}}\left(a_z\varphi\frac{\partial\psi}{\partial\tilde{r}}\right)\right]$$
$$-\tilde{r}\frac{\partial}{\partial z}\left(F\cdot b_\varphi\frac{\partial\varphi}{\partial z}\right) - a_r\frac{\partial}{\partial\tilde{r}}\left(\tilde{r}b_\varphi\frac{\partial\varphi}{\partial\tilde{r}}\right) - Fa_z\left[\frac{\partial}{\partial\tilde{r}}\left(\tilde{r}b_\varphi a_z\frac{\partial\varphi}{\partial\tilde{r}}\right)\right.$$
$$\left. + \frac{\partial}{\partial\tilde{r}}\left(\tilde{r}b_\varphi\frac{\partial\varphi}{\partial z}\right)\right] - \frac{\partial}{\partial z}\left(\tilde{r}Fb_\varphi a_z\frac{\partial\varphi}{\partial\tilde{r}}\right) + \tilde{r}Fd_\varphi = 0. \tag{3.2}$$

Here

$$a_r = \frac{1}{F(z)}, \quad a_z = -\frac{\tilde{r}F'(z)}{F(z)} \tag{3.3}$$

and the functions φ, a_φ, b_φ and d_φ are listed in Table 1.

Table 1

φ	a_φ	b_φ	d_φ
$\frac{\omega}{\tilde{r}}$	$\tilde{r}^2$	$\frac{\tilde{r}^2}{\mathrm{Re}}$	$\frac{\mathrm{Gr}}{\mathrm{Re}^2}\tilde{r}^2\frac{\partial\theta}{\partial\tilde{r}}$
ψ	0	$\frac{1}{\tilde{r}^2}$	$-\frac{\omega}{\tilde{r}}$
θ	1	$\frac{1}{\mathrm{RePr}}$	0

Equation (3.2) and the boundary conditions (2.4)–(2.7) are approximated by employing the finite difference form obtained for the equation by integrating it over a control volume around every grid point. A grid system of 21×41 grid points was used to cover a half of the zone that is symmetrical about the axis. The corresponding nonlinear algebraic system is solved by iteration. Convergence was tested by the difference of computed values of each parameter in the successive iterations.

Equation (2.8) for the zone shape is solved by successive integrations starting from the exact solution for the zone with a very large radius compared with its length.

4. Results

The convection flow pattern and temperature field in the zone are calculated for radiant heating which is approximated by taking a parabolic temperature profile along the melt surface

$$\tilde{\theta} = 1 - z^2. \tag{4.1}$$

It is supposed that $R = L = 2 \cdot 10^{-3}$ m ($A = 1$). The calculations are carried out for molten silicon (Si) and sodium nitrate ($NaNO_3$). For the physical properties of silicon

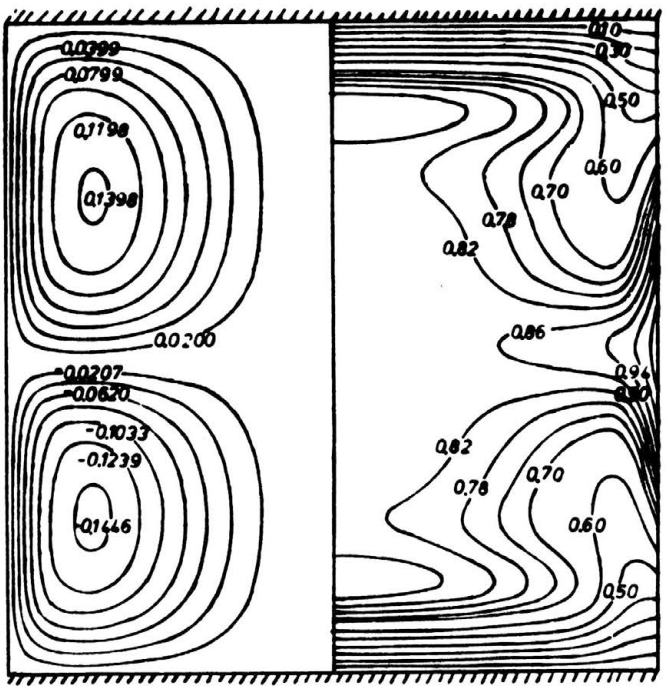

$Ma = 63.848$ $\quad Bo_{dyn} = 0.036$

$Pr = 0.023$ $\quad \Delta T = 1\text{K}$

FIG. 2.

near the melting point, namely, $\varrho = 2.5 \cdot 10^3\ \mathrm{kg\,m^{-3}}$, $\nu = 3.52 \cdot 10^{-7}\ \mathrm{m^2 s^{-1}}$, $\chi = 1.53 \times$ $\times 10^{-7} \mathrm{m^2 s^{-1}}$, $\beta = 1.6 \cdot 10^{-4}\ \mathrm{K^{-1}}$, $\sigma = 7.2 \cdot 10^{-1}\ \mathrm{N\,m^{-1}}$, $\alpha = 4.3 \cdot 10^{-4}\ \mathrm{Nm^{-1}K^{-1}}$, the numbers are as follows: $\mathrm{Bo_{dyn}} = 0.036$, $\mathrm{Bo_{stat}} = 0.136$ and $\mathrm{Pr} = 0.023$ [14]. The Marangoni number additionally depends on the temperature difference and changes linearly with it. For $\Delta T = 1$ K and 10 K the number Ma is equal to 63.848 and 638.48, respectively. The numerical results for the cylindrical zone of molten silicon are presented in Figs. 2 and 3. The stream lines are drawn in the left half of the figure and the isoterms are in the right half.

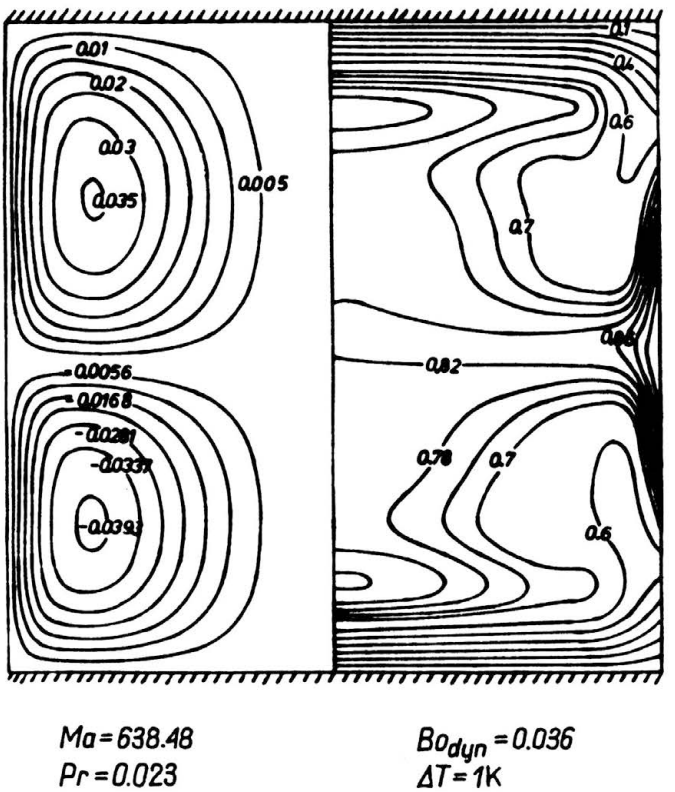

FIG. 3.

There are only two toroidal convection rolls for the temperature differences considered. It is obvious that the gravity has a negligible effect on the liquid motion and the temperature distribution. The upper roll is a little stronger than the lower one because the former is driven by combined surface tension and buoyant forces near the free sufrace while in the latter both forces act in opposite directions. The temperature field is approximately symmetrical about the middle equator plane. It depends strongly on the convection. The role of convection increases with the temperature differences, i.e. when the Marangoni number grows.

There is a layer on each rigid wall in which the temperature increases from zero to

some maximum value in the z direction away from the rods. The temperature field is nearly homogeneous out of the layers in the zone core.

The convection heat transfer has a considerable effect on the temperature distribution for larger Prandtl numbers, as it is seen in Fig. 4 showing the results for sodium nitrate

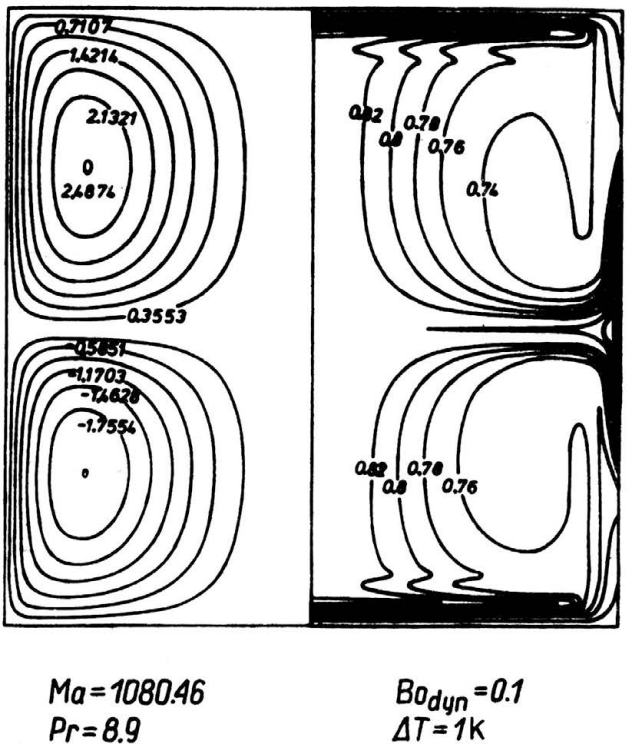

FIG. 4.

($\varrho = 1.904 \cdot 10^3$ kg m^{-3}, $\nu = 1.48 \cdot 10^{-6}$ m^2 s^{-1}, $\chi = 1.67 \cdot 10^{-7}$ m^2 s^{-1}, $\beta = 1 \cdot 10^{-4}$ K^{-1}, $\sigma = 1.2 \cdot 10^{-1}$ N m^{-1}, $\alpha = 7 \cdot 10^{-5}$ N m^{-1} K^{-1}, Pr = 8.9, $\mathrm{Bo}_{\mathrm{dyn}} = 0.1$ and Ma = = 1080.46 for $\Delta T = 1$ K [6]). The isoterms in the zone core are very similar to the stream lines, so the heat transfers mainly by the fluid motion.

The results obtained here are in good qualitative agreement with some experimental data [8, 13] and numerical solutions for cylindrical zones [17–19].

The calculations for an axisymmetric zone with a quasi-equilibrium shape were also performed. Typical results for silicon are shown in Fig. 5. The shape is determined for $\gamma_1 = 1.4$ rad and $\gamma_2 = 1.3$ rad. These values of the contact angles approximate those observed in the experiments reported in [8] (see Fig. 6 taken from that paper). For these angles and $A = 1$ the upper rod radius occurs to be equal to the radius of the lower one. Comparing the stream lines in Figs. 2 and 5 obtained at the same conditions, one can conclude that there is a little visible difference between them. The vortex centers in the axisymmetric case are only shifted to the domain corners. But the vortex strength really increases almost twice and, as a result, the warmer portions of the liquid near the equator are carried more

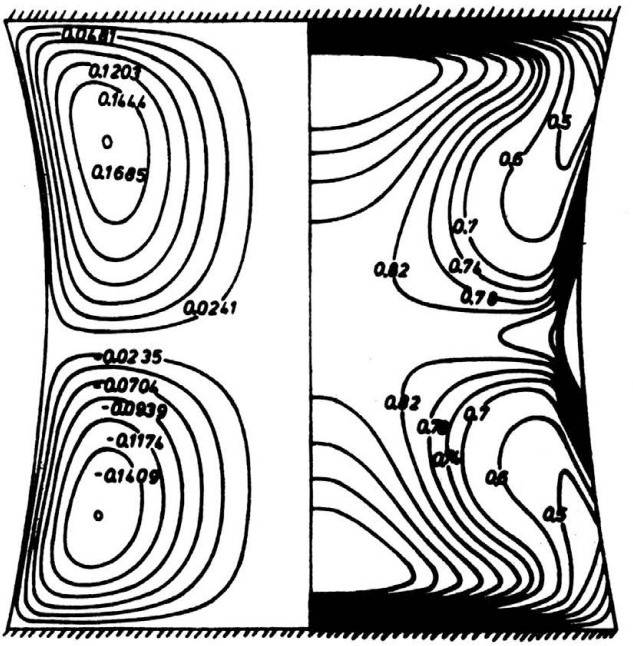

FIG. 5.

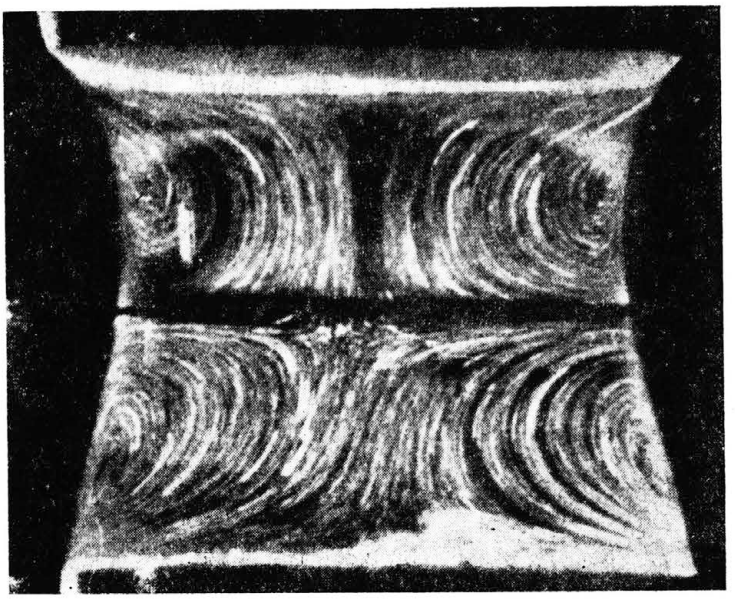

FIG. 6.

intensively along the free surface and the rod wall. This leads to a considerable change in the temperature field. The thickness of the temperature layers decreases about twice. Moreover, two domains of maximum temperatures are formed just out of the layers and the central core of homogeneous temperature is pressed.

The flow patterns are very similar to those presented in Fig. 6. We expect that the forthcoming calculations for larger zones and temperature differences will confirm quantitatively the experimental data.

References

1. W. G. PFANN, *Zone melting*, John Wiley and Sons, New York 1966.
2. J. R. CARRUTHERS, M. GRASSO, J. Appl. Phys., **43**, p. 436, 1972.
3. D. SCHWABE, A. SCHARMANN, F. PREISSER, R. OEDER, J. Crystal Growth, **43**, p. 305, 1978.
4. D. SCHWABE, A. SCHARMANN, J. Crystal Growth, **46**, p. 125, 1979.
5. D. SCHWABE, A. SCHARMANN, F. PREISSER, in: Proc. of 3rd European Symp. on Material Sciences in Space, Grenoble, ESA SP-142, p. 9, 1979.
6. D. SCHWABE, A. SCHARMANN, F. PREISSER, Acta Astronautica, **9**, p. 183 and 265, 1982.
7. C.-H. CHUN, W. WUEST, in: COSPAR Space Research, Eds. M. J. RYCROFT, A. C. STICKLAND, **18**, p. 523, 1978.
8. C.-H. CHUN, W. WUEST, Acta Astronautica, **5**, p. 681, 1978.
9. C.-H. CHUN, W. WUEST, Acta Astronautica, **6**, p. 1073, 1979.
10. W. WUEST, C.-H. CHUN, in: COSPAR Space Research, ed. M. J. RYCROFT, **19**, p. 559, 1979.
11. C.-H. CHUN, W. WUEST, Acta Astronautica, **7**, p. 479. 1980.
12. C.-H. CHUN, J. Crystal Growth, **48**, p. 600, 1980.
13. C.-H. CHUN, in: *Microgravity fluid dynamics. Foundations and applications*, CISM, Udine, Italy, June 29 — July 3, 1981.
14. CH. E. CHANG, W. R. WILCOX, J. Crystal Growth, **28**, p. 8, 1975.
15. CH. E. CHANG, W. R. WILCOX, Int. J. Heat Mass Transfer, **19**, p. 355, 1976.
16. CH. E. CHANG, J. Crystal Growth, **44**, p. 168, 1978.
17. CH. E. CHANG, W. WILCOX, R. A. LEFEVER, Mater. Res. Bull., **14**, p. 527, 1979.
18. P. A. CLARK, W. R. WILCOX, J. Crystal Growth, **50**, p. 461, 1980.
19. W. WUEST, in: *Microgravity fluid dynamics. Foundations and applications*, CISM, Udine, Italy, June 29 — July 3, 1981.
20. N. KOBAYASHI, W. R. WILCOX, Crystal Growth, **59**, p. 616, 1982.
21. B. YA. MARTUZAN, E. N. MARTUZANE, ICCG-6, Poster 363, Extended Abstracts, II, p. 246, Moscow 1980.
22. H. WILKE, ZAMM, **60**, p. 437, 1980.
23. D. SCHWABE, Phys. Chem. Hydrodyn. **2**, p. 263, 1981.
24. A. GOSMEN *et al.*, *Heat and mass transfer in recirculating flows*, Academic Press, London and New York 1969.
25. S. R. CORIELL, M. R. CORDES, J. Crystal Growth, **42**, p. 466, 1977.
26. *Hydrodynamics at zero gravity*, Ed. by A. D. MISHKIS, 1976 [in Russian].

INSTITUTE OF MECHANICS AND BIOMECHANICS, BAS, BULGARIA.

Received September 14, 1983.